AIP Journal of Applied Physics

Transient and steady state photorefractive responses in dye-doped nematic liquid crystal cells

Prapong Klysubun and Guy Indebetouw

Citation: Journal of Applied Physics **91**, 897 (2002); doi: 10.1063/1.1427431
View online: http://dx.doi.org/10.1063/1.1427431
View Table of Contents: http://scitation.aip.org/content/aip/journal/jap/91/3?ver=pdfcov
Published by the AIP Publishing

Transient and steady state photorefractive responses in dye-doped nematic liquid crystal cells

Prapong Klysubun and Guy Indebetouw[a)]
Department of Physics, Virginia Tech, Blacksburg, Virginia 24061-0435

(Received 6 July 2001; accepted for publication 19 October 2001)

The photorefractive response of several dye-doped nematic liquid crystal samples is studied experimentally. Particular attention is given to the observation and modeling of the multiexponential dynamics of the photorefractive grating, and of the photocurrent. Both involve at least two different mechanisms with largely different time constants. These phenomena occur on time scales on the order of seconds, for applied voltages about 1 V, and light intensities as low as milliwatts/cm^2.
 [DOI: 10.1063/1.1427431]

I. INTRODUCTION

Photorefractive materials have been, and continue to be actively studied for their potential applications in, e.g., optical storage and information processing.[1] Inorganic materials are developed for applications requiring stability and long lifetimes, while organics offer unique attributes of flexibility and recyclability. The most promising organic photorefractive materials are based on polymers, liquid crystals, or a combination of both (e.g., polymer-dispersed liquid crystals, polymer-stabilized liquid crystals). In all these materials, molecular reorientation is the main photorefractive mechanism, and is responsible for their large photoinduced response.[2–7]

Liquid crystals are attractive because they exhibit large photoinduced anisotropy, and require only very small external fields to change their properties significantly.[8] Typically, a photorefractive response in liquid crystals requires a field of 1/10 V/μm, in contrast with the several hundreds of V/μm required by polymers. In addition, a large variety of liquid crystals with different physical and chemical properties have been developed for display applications and are readily available at low cost. An excellent review of recent work in photorefractive liquid crystals has been published recently.[9]

The interest in liquid crystals as electro-optic and photo-optic materials has increased further when it was realized that the photoinduced effects could be enhanced by orders of magnitude with the addition of minute amounts of absorbing dyes.[10–13] Molecular models have been developed describing this large response of dye-doped liquid crystals.[14–18] However, the details of the microscopic mechanisms involved are still not entirely understood, and quite often, experimental results still reveal unexpected behaviors.

The main goal of this article is to report the observation of the occurrence of two different photorefractive gratings in dye-doped nematic liquid crystals. One is a transient grating occurring on a time scale of a few seconds. The other occurs on a longer time scale of several tens of seconds, and leads to a steady state response. Photorefractivity in liquid crystals may result from several physical mechanisms with different time constants[9] (e.g., ion diffusion, conductivity and/or dielectric anisotropy, director reorientation, and surface director alignment). Transient responses have also been reported, and are to be expected in low viscosity systems.[8] Two- and four-wave mixing experiments were carried out to identify the nonlocal photorefractive nature of both gratings. Two time scales of comparable orders of magnitude were also identified in the photocurrent buildup dynamics of these samples. Furthermore, a strong transient photoinduced birefringence was also observed, and may bear some relationship to the transient photorefractive response reported here. These results are reported in Sec. III. Section II briefly summarizes the results of measurements of the photorefractive response, two-beam energy exchange, and diffraction efficiency in the steady state regime, for a number of liquid crystal/dye combinations. These results are not entirely new, but they confirm data reported by others, and help characterize the systems used in this study.

II. STEADY STATE TWO-WAVE MIXING

The samples were made using several nematic liquid crystals and liquid crystal mixtures from Merck [namely, E7, E44, K15 (5CB), and others], and different dyes including disperse red DR1 and disperse orange DO25. The dye concentrations were varied between 0.20% and 0.60% in weight. The mixtures were introduced between two glass plates coated with indium–tin–oxide electrodes. For all the samples discussed here, Mylar® or Teflon™ spacers held the plates 25 μm apart. Prior to introducing the liquid crystal mixture, the plates were treated with the surfactant octadecyltrichlorosilane to induce a homeotropic alignment. The homogeneity of the alignment was checked under a microscope.

In the two-wave mixing experiments, the samples were excited by the interference of two beams from a continuous-wave diode-pumped frequency-doubled Nd: Yttrium–aluminum–garnet laser operating at 532 nm. The two beams with a diameter of 2.25 mm (at e^{-2} intensity) overlapped in the sample with a small angle between them. The angle of incidence on the sample was about 45° for all the experi-

[a)]Author to whom correspondence should be addressed; electronic mail: gindebet@vt.edu

ments. The polarization of the two interfering beams was parallel to the plane of incidence (extraordinary waves). This was found to be a necessary condition for observing a photorefractive response.

Energy exchange in two-wave mixing, where one of the transmitted beams experiences a gain of energy while the other experiences a corresponding loss, has been used as a way of identifying the nonlocal nature of the photorefractive response of a material. In the experiment, the power of the two transmitted beams were monitored by two photodetectors. The standard theory of photorefraction[1,19] gives the following expression for the intensity of the transmitted beams in the Bragg (thick grating) regime:

$$I_{1(2)}(z)=I_{1(2)}(0)\frac{[1+m^{-(+)1}]\exp(-\alpha z)}{1+m^{-(+)1}\exp[+(-)\gamma z]}, \tag{1}$$

where $m=I_1(0)/I_2(0)$ is the beam intensity ratio at the entrance face of the cell, α is the linear absorption coefficient, and γ is the exponential gain coefficient. The gain coefficient is the real part of the complex coupling coefficient Γ given, in terms of the refractive index modulation Δn, as $\Gamma=ik(\cos\theta)^{-1}\Delta n\exp(-i\Phi)$. Here, $k=2\pi/\lambda$ is the wave number, θ the angle of incidence, and Φ is the spatial phase shift between the periodic interference pattern (the excitation pattern) and the resulting refractive index modulation (the grating response). $\Phi\neq 0$ is indicative of a nonlocal response, a necessary condition to observe any energy exchange between the two beams. The energy exchange is maximum when $\Phi=\pi/2$. Experimentally, the gain coefficient is measured by monitoring the intensity of the two transmitted beams and using the relationship

$$\gamma=\frac{\cos\theta}{d}\ln\left[\frac{I_2/I_{20}}{I_1/I_{10}}\right], \tag{2}$$

where d is the sample thickness, $I_{1(2)}$ is the transmitted intensity of the beam experiencing loss (gain) with the applied voltage V_a applied across the cell, and $I_{10(20)}$ is the corresponding transmitted intensity without the applied voltage. In all the following experiments $I_{10}=I_{20}$.

Equations (1) and (2) are derived in the Bragg (thick grating) regime, where the wave equation in the medium can be separated into a pair of coupled equations, one for each interacting beam. The validity of these equations in the Raman–Nath (thin grating) regime, characterized by the presence of multiple diffraction orders, is questionable.[9] As suggested in Ref. 9, a simpler parameter to characterize two-beam-coupling strength could be the intensity ratio of the beams. Such a parameter is independent of sample thickness, and is directly accessible experimentally. One can define, for each beam, the ratio of the transmitted intensity to the incident intensity, or one can compare the intensity ratio of the two beams before and after their interaction. In all the experiments reported here, the incident beam intensity ratio is equal to unity. We thus chose to characterize our experimental results in terms of the beam intensity ratio exiting the sample. The sample absorption is not included in this parameter. The gain coefficient, however, has been almost exclusively used in the past, and is still used by a number of authors, even for very thin samples. For this reason, we are also giving the values of the gain coefficient calculated with Eq. (2), knowing that its interpretation as an exponential gain coefficient becomes invalid in the thin grating regime.

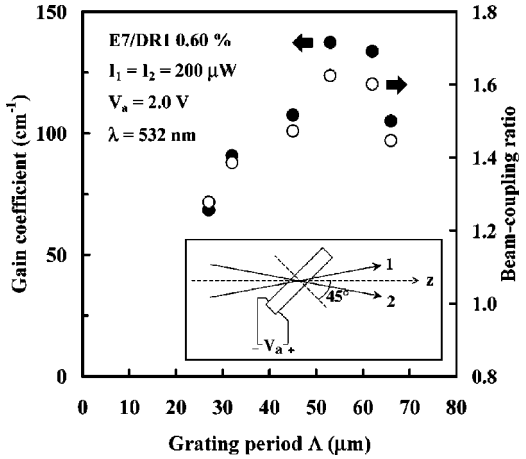

FIG. 1. Measured beam-coupling intensity ratio (I_2/I_1) for an incident intensity ratio equal to unity, and calculated gain coefficient, as functions of the grating period for the sample E7/DR1 0.60 wt %. (Inset) Two-beam coupling geometry and sign convention.

The measured beam-coupling intensity ratio I_2/I_1 for an incident ratio equal to one, as well as the calculated gain coefficient, for the sample E7/DR1 0.60 wt. % as functions of the period of the interference pattern is shown in Fig. 1. The input intensities were $I_{10}=I_{20}=100\,\mu$W, and the applied voltage was $V_a=2.0$ V across the 25 μm cell. The inset in Fig. 1 defines the geometry of the interaction and the sign convention adopted in the article. Figure 1 shows a maximum response for a grating period about twice the sample thickness, as has been reported by others.[20]

Figure 2 shows the beam-coupling ratio, and the calculated gain coefficient as functions of the applied voltage for the sample E7/DR1 0.20 wt. %. The input intensity is 100 μW for each beam, and the grating period is 50 μm. The gain/loss coefficients of each interacting beam are plotted separately. The geometry is that shown in the inset of Fig. 1. There is an apparent threshold at about ± 1 V, and saturation sets in around ± 3 V, a voltage beyond which significant scattering occurs. Samples with higher dye concentration (larger than $\sim$0.50 wt. %) exhibited an onset of dynamic scattering at voltages above about 2–2.5 V. At these high concentration levels, a marked field-asymmetric response was also noted. This can presumably be attributed to asymmetric scattering phenomena similar to the fanning effect prominent in organic and inorganic materials with large photorefractive gain.[21,22] These adverse effects may be related to the fairy strong absorption of the dye DR1 at the laser wavelength (532 nm). They were much less pronounced in samples containing the dye DO25 whose absorption coefficient was less than half that of DR1 at that wavelength.

The threshold around 1 V and the saturation around 3 V correspond to the threshold for the onset of the photocurrent and for its saturation, respectively. The photocurrent was measured with a picoammeter, and with sample excitation at 532 nm. It was found to vary nearly linearly with the intensity of the input beam, as shown in Fig. 3 for the sample

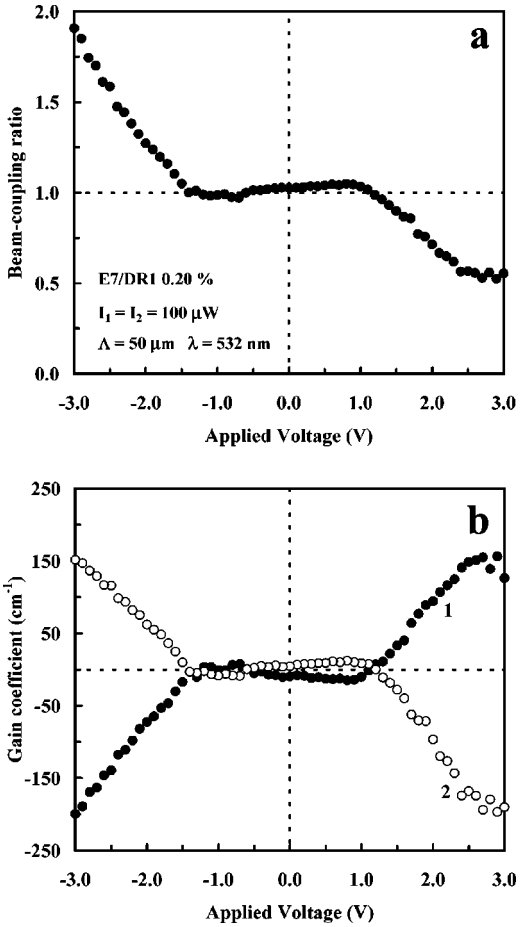

FIG. 2. Beam-coupling ratio (a), and gain/loss coefficients for each beam (b), as functions of the applied voltage for the sample E7/DR1 0.20 wt %. The geometry is defined in the inset of Fig. 1.

E7/DR1 0.40 wt. %. For an applied voltage of 2.5 V and a beam diameter 2.25 mm, the rate is about $I_{\mathrm{ph}} \sim (1.45\,\mu\mathrm{A/W}) I^{0.9}$, where I is the beam power in W. A linear relationship is indicative of a carrier recombination rate proportional to their density. The dark current versus applied voltage relationship ($I-V$ curve) for the E7/DR1 0.60 wt. % sample is shown in Fig. 4. From 0.2 to about 0.75 V, the current varies by 2 orders of magnitude following a power

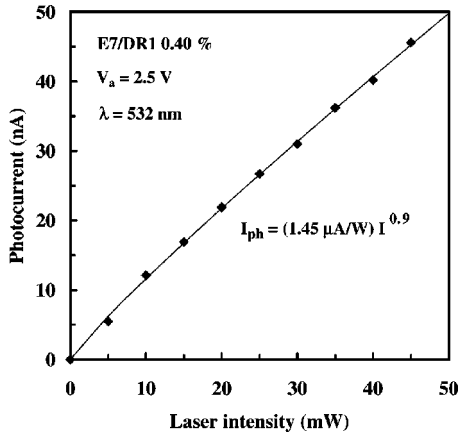

FIG. 3. Photocurrent as a function of the laser beam power (diameter 2.25 mm) for the sample E7/DR1 0.40 wt %.

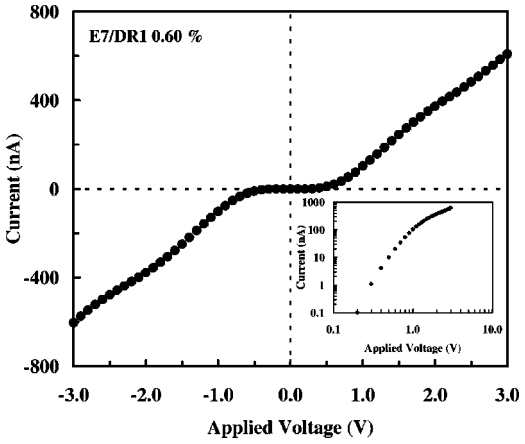

FIG. 4. $I-V$ curve of the sample E7/DR1 0.60 wt %. (Inset) $I-V$ log–log plot.

law $I(V) \propto V^3$, as shown on a log–log scale in the inset. Between about 1 and 2 V, the relationship is nearly ohmic, with a conductance $\rho_{\mathrm{dark}} \sim 275$ nA/V. From 2 to 3 V, a region in which scattering increases significantly, the conductivity drops to ~235 nA/V. The increase in the conductivity beyond $V_a \sim \pm 0.7$ V presumably originates from the field ionization of the dye molecules and impurities in the liquid crystal host.[23] Figure 5 shows the photocurrent as a function of the applied voltage, together with a fit to $I_{\mathrm{ph}} \sim \rho_{\mathrm{ph}}(V_a - V_{\mathrm{th}})$. The photocurrent was calculated as the difference between the total current through the illuminated sample and the dark current. The sample was illuminated by a 30 mW, 532 nm beam with a 2.25 mm diameter. There is a marked threshold around 1.5 V, a voltage nearly equal to that of the two-beam coupling gain threshold (Fig. 2). Above that threshold, the photocurrent grows linearly with a photoconductance $\rho_{\mathrm{ph}} \sim 65$ nA/V. This threshold behavior is similar to that observed in undoped liquid crystal.[24]

The two-beam coupling intensity ratio was measured for a number of liquid crystal/dye combinations as a function of the beam power. Representative results are shown in Fig. 6.

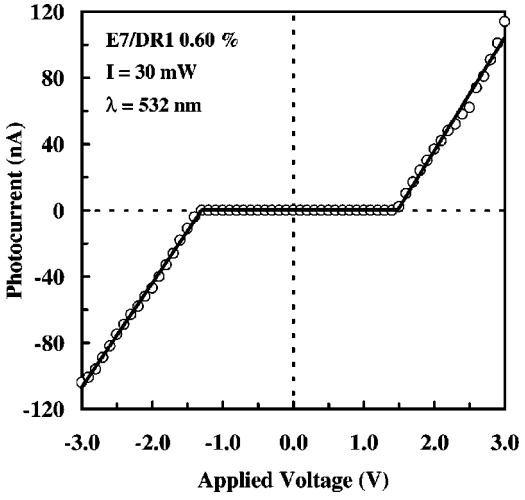

FIG. 5. Photocurrent as a function of the applied voltage for the sample E7/DR1 0.60 wt % under 30 mW beam power illumination (beam diameter 2.25 mm).

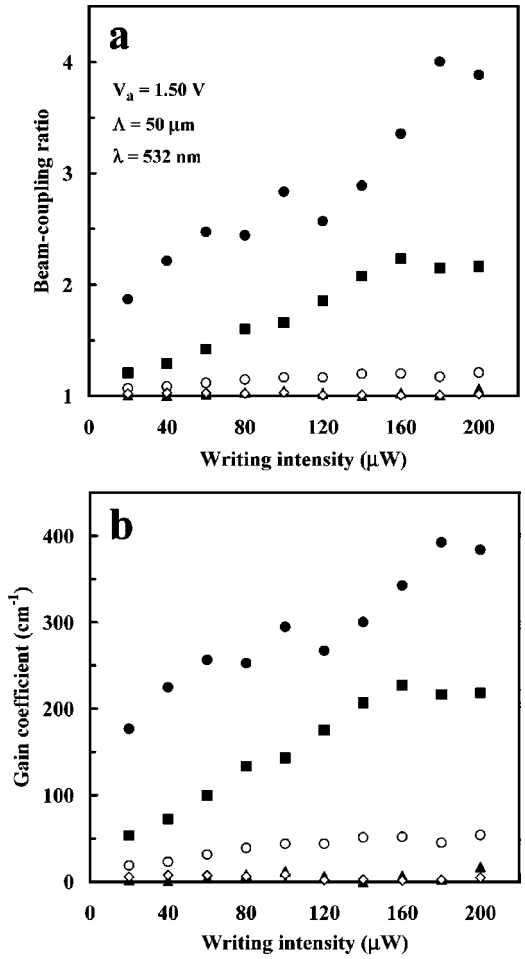

FIG. 6. Beam-coupling ratio for incident intensity ratio equal to unity (a), and calculated gain coefficient (b), as functions of the beam power for several liquid crystal/dye combinations: (solid circles) E7/DO25, (solid squares) E44/DR1, (opened circles) E7/DR1, (opened diamonds) K15/DO25, (solid triangles) MLC-6204-000/DR1. Sample thickness: 25 μm, dye concentration: 0.40 wt %.

All samples had the same thickness (25 μm) and the same concentration (0.40 wt. %). The applied voltage was 2.0 V, the incidence angle 45°, and the grating period was 50 μm. The absorption coefficient at 532 nm was about 250 cm^{-1} for E7/DR1, and 100 cm^{-1} for E7/DO25. The results of Fig. 6 illustrate the wide range of responses that can be obtained with liquid crystal/dye mixtures, as has been observed by others and as theory predicts.[25–28]

Strong absorption in two-beam coupling experiments may complicate matters. For this reason, the grating response was also probed by observing the diffraction of a weak 633 nm beam from a He–Ne laser, a wavelength at which the samples absorb negligibly. The diffraction efficiency was found to vary linearly with the writing beam intensity. For the sample E7/DR1 0.40 wt. %, and an applied voltage of 2.0 V, the rate measured in Fig. 7 is about $\eta \sim 10^{-2}\,\mathrm{W}^{-1}$ (i.e., 2% of incident 633 nm light diffracted by a grating induced by two 532 nm beams of 200 μW each). This leads to a refractive index modulation approaching 10^{-3}, which is comparable to what has been achieved with polymeric materials.

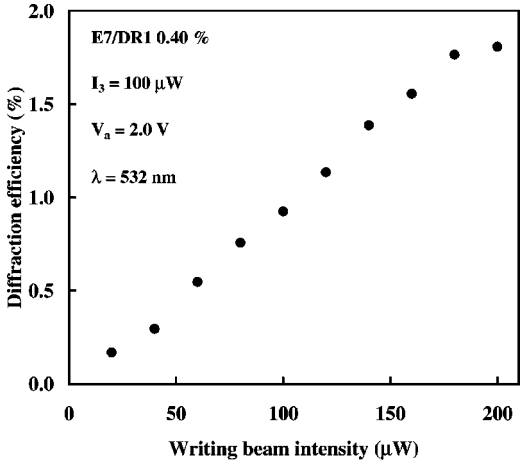

FIG. 7. Diffraction efficiency as a function of the writing beam power (equal incident power) for the sample E7/DR1 0.40 wt %.

III. DYNAMIC RESPONSE

A typical grating buildup and decay dynamics is shown in Fig. 8. This shows the diffraction efficiency of a weak 633 nm probe beam by a grating induced by the interference of two 532 nm beams intersecting at a small angle in the sample. For Fig. 8, the sample was E7/DR1 0.60 wt. %, the period of the interference pattern was 60 μm, the incidence angle 45°, the incident beam intensities were $I_1 = I_2 = 200\,\mu$W, and the applied voltage was 2.00 V. One can clearly identify a relatively fast transient buildup (and decay) superposed to the expected monotonic exponential growth (and decay) of the grating. The procedure leading to these results was the following. The voltage was first applied to the sample for several minutes. One of the writing beams and the probe beam were then turned on. The probe beam was chopped for synchronous detection. After all transients had settled, the second writing beam was turned on, creating the interference pattern and inducing the photorefractive grating. The first-order diffraction of the probe beam was monitored with a photomultiplier, and measured through a lock-in am-

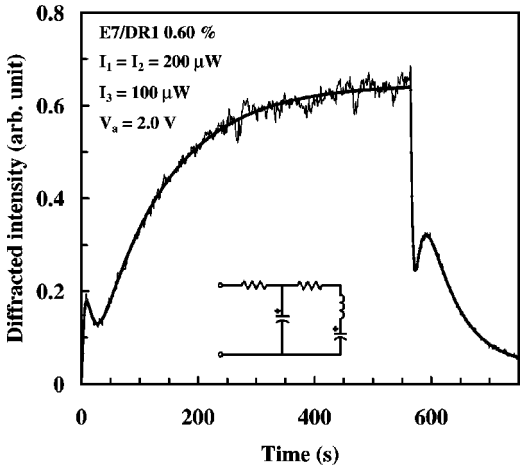

FIG. 8. Typical grating buildup and decay dynamics induced by the interference of two 532 nm beams (200 μW power each), calculated from the diffraction of a weak 633 nm probe. (Inset) equivalent circuit with a triple-exponential response used to fit the data.

plifier. The buildup and decay of Fig. 8 can be modeled quite accurately by an equivalent circuit (Fig. 8 inset) that includes a slow capacitive component τ_1 and a faster reactive component τ_2 with an overall low pass τ_3. The step response of such a circuit is represented as

$$h(t) \propto \{A[1-\exp(-t/\tau_1)] + B\exp(-t/\tau_2)\} \times H(t) * \exp(-t/\tau_3)H(t), \quad (3)$$

where $*$ represents a convolution, and $H(t)$ is a Heaviside step function. Such a response is measured as a three exponential with time constants τ_1, τ_2, and τ_3. Indeed, the buildup dynamics of Fig. 8 can be fitted as

$$I_{\mathrm{up}}(t) = I_\infty[1 - a_1\exp(-t/\tau_1) - a_2\exp(-t/\tau_2) - a_3\exp(-t/\tau_3)]. \quad (4)$$

With the constraint $a_1+a_2+a_3=1$, we find $\tau_1 \sim 120\,\mathrm{s}$, $\tau_2 \sim 10\,\mathrm{s}$, $\tau_3 \sim 7\,\mathrm{s}$, and $a_1=1.1$, $a_2=-2.2$, and $a_3=2.1$. From Eqs. (3) and (4), we find a ratio $B/A \approx 2/3$ between the reactive and capacitive components. Similarly, the step down response is

$$h'(t) = A'[1-H(t)] + [A'\exp(-t/\tau_1') - B'\exp(-t/\tau_2')]H(t) * \exp(-t/\tau_3')H(t), \quad (5)$$

and the decay dynamics of Fig. 8 is modeled as

$$I_{\mathrm{down}}(t) - b = I_0[a_1'\exp(-\tau/\tau_1') + a_2'\exp(-t/\tau_2') + a_3'\exp(-t/\tau_3')], \quad (6)$$

where b is a constant background, which could be attributed to a quasipermanent modulation of the director at the anchoring surfaces. With the constraint $a_1'+a_2'+a_3'=1$, we find $\tau_1' \sim 50\,\mathrm{s}$, $\tau_2' \sim 12\,\mathrm{s}$, $\tau_3' \sim 4\,\mathrm{s}$, $a_1'=0.9$, $a_2'=-1.2$, and $a_3'=1.3$. This fit gives the same ratio $B'/A' \approx 2/3$. The main difference between the buildup and the decay dynamics is that the capacitive decay time constant is only about half the corresponding buildup time constant. Nevertheless, it is interesting to observe that the relative strengths of the three mechanisms, as measured by their fractional area under the response curve ($f_i \propto a_i\tau_i$), are approximately in the same ratios for the buildup as for the decay dynamics, namely, $f_1:f_2:f_3 \approx 1:0.2:0.1$.

The buildup and decay dynamics of the photorefractive response was also monitored by recording the intensities of the two transmitted writing beams in a two-beam coupling mode. This was done in order to identify the nature of both the transient and the steady state gratings. The temporal evolution of the transmitted beams for the sample E7/DR1 0.6 wt. %, shown in Fig. 9, exhibits the same transient behavior superposed on an exponential buildup. The nature of the transient and the steady state gratings was probed using the grating translation technique.[29–31] The phase of one of the interfering beams is varied rapidly over a multiple of 2π. This was done by translating a mirror with a piezoelectric activator. During the translation, the grating amplitude does not decay significantly, and the intensity of the transmitted beams vary cyclically, as the direction of energy exchange follows the phase of the grating relative to that of the interference pattern. The two signals can be processed to determine with reasonable confidence the magnitude of the absorption component and the phase component of the grating as well as the relative phase Φ between the interference pattern and the induced grating.[32,33] The grating translation technique was applied first shortly after the turnon of the second beam, when the transient grating dominates, and the steady state grating has not reached a significant amplitude yet. This is indicated by arrow A in Fig. 9. The resulting signal modulation is shown in the inset. The technique was again repeated after the transient grating had disappeared and a steady state was reached (arrow B and corresponding inset in Fig. 9). In both cases it was determined unambiguously that both gratings are nearly pure phase gratings, and that the relative phase between the grating and the interference pattern is very close to $\pi/2$ in both cases. This, together with other observations, leads us to identify the source of the periodic refractive index change as reorientation of the dye driving the local orientation of the local liquid crystal director in the combined external and space-charge fields, thus leading to a periodic modulation of birefringence lagging the incident intensity modulation by $\pi/2$.

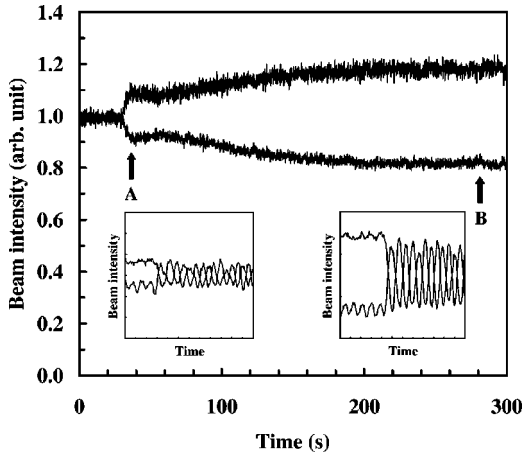

FIG. 9. Typical buildup of the energy exchange between the two interacting 532 nm beams. The grating phase shift is measured at the two instants indicated by the arrows, using the grating translation method (result shown in the two insets).

IV. PHOTOCURRENT AND TRANSIENT BIREFRINGENCE

In an effort to correlate the transient and steady state photorefractive responses observed in these samples with other physical parameters, a number of different tests were carried out. Two of them are worth mentioning, as they may bare some relationship to the reported observations.

Photorefractivity involves the photoexcitation of charges and their transport. There is a direct correlation between photoconductivity and photorefractivity.[9] The photocurrent through sample E7/DR1 0.40 wt. % was measured with a picoammeter when an expanded beam from an argon laser was incident on the sample at near normal incidence. This beam had a power of about 80 mW, a diameter of 9 mm, and a wavelength of 514 nm. A voltage of 2.0 V was first applied across the sample. After a couple of minutes, a shutter was

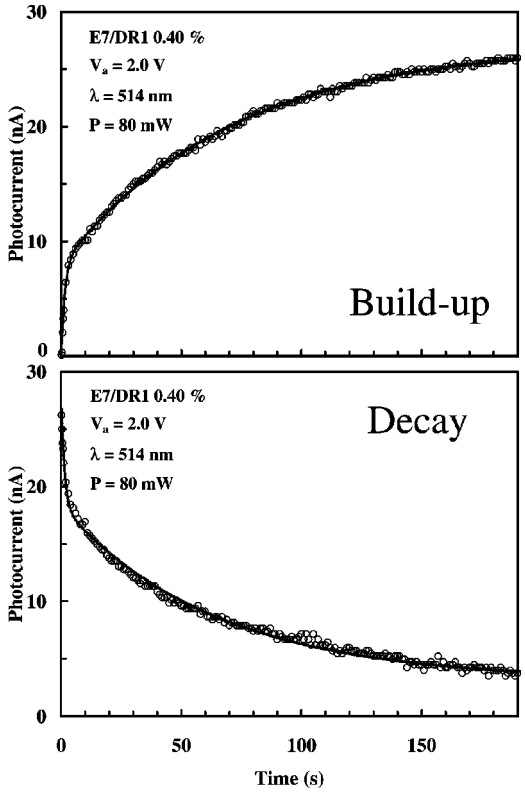

FIG. 10. Typical buildup and decay of the photocurrent showing two distinct time constants.

opened, and the additional photocurrent through the illuminated sample was monitored with a picoammeter. Again, as shown in Fig. 10, two distinct time constants can be identified in the buildup and the decay dynamics. These were fit to the following expressions:

$$J_{\mathrm{up}}(t) \propto 1 - a_1 \exp(-t/\tau_1) - a_2 \exp(-t/\tau_2), \tag{7}$$

with the constraint $a_1 + a_2 = 1$ for the buildup, and

$$J_{\mathrm{down}}(t) - b \propto a_1' \exp(-t/\tau_1') + a_2' \exp(-t/\tau_2'), \tag{8}$$

with the constraint $a_1' + a_2' = 1$ for the decay. We find $\tau_1 = 70\,\mathrm{s}$, $\tau_2 = 1.4\,\mathrm{s}$, $a_1 = 0.3$, and $a_2 = 0.7$ for the buildup, and $\tau_1' = 60\,\mathrm{s}$, $\tau_2' = 1.3\,\mathrm{s}$, $a_1' = 0.4$, and $a_2' = 0.6$ for the decay. The long-lived tail represented by the parameter b could be due to a change of dark conductivity. The dark conductivity in these samples is typically 1 order of magnitude larger than the photoconductivity, as for most polymeric materials ($J_{\mathrm{ph}}/J_{\mathrm{dark}} \sim 0.2$ in this experiment). These time scales and behavior depend only weakly on the intensity of the excitation.

Another transient phenomenon that may bare some relationship to the reported observations is the strong transient birefringence measured in these samples. In organic materials, and certainly in liquid crystals, the photorefractive response is dominated by molecular orientational effects. It is thus directly related to the local birefringence of the material. The photoinduced birefringence was monitored by sending a weak probe beam (He–Ne laser, 633 nm, diameter ~1.5 mm) polarized at 45° with the plane of incidence through the central region of the sample excited by the expanded beam from an argon laser (wavelength 514 nm, diameter ~9 mm). The probe beam incidence angle was about 45° with the sample normal. After transmission through the sample, the *s* and *p* waves, respectively, polarized perpendicular and parallel to the plane of incidence, were separated by a polarization beam splitter, and the two components were monitored by two separate photodetectors. The following was observed. Upon application of the excitation beam, the *s* and *p* components experience large transient variations with opposite signs. The total energy transmitted remains constant, which points toward a purely orientational effect. Interestingly, the effect does not depend on the polarization of the excitation beam. This transient response is different from the transient birefringence reported in Ref. 34, which occurs with a time scale shorter, by more than 1 order of magnitude, and results from different interaction geometry. The transmitted intensity of the *s* and *p* waves, without photoexcitation, are strongly dependent on the incident angle of the probe beam. This is simply a result of the homeotropic alignment of the cell, and the strong birefringence of the liquid crystal. Individually, the *s* and *p* waves are transmitted through the cell without change of polarization, and this remains true after application of the excitation beam. This means that the *s* and *p* waves, are and remain the ordinary and extraordinary eigenpolarization state of the sample. Thus, the principal axes of the birefringent sample do not change, indicating that the observed transient rotation of the director occurs within the plane of incidence.

Strong polarization gratings have also been induced in these samples, using two incident beams with orthogonal polarizations. The illumination of the sample is then spatially uniform in intensity, but the polarization state is spatially modulated. Consequently, such an excitation probes only the orientational response of the sample to the polarization state of the optical field. Details of these results will be reported elsewhere.

V. SUMMARY

The large photoinduced response of dye-doped nematic liquid crystals has renewed interest in these systems, both theoretically, and experimentally. The observation of a nonlocal photorefractive response in these samples is of particular interest for their possible applications in optical storage, information processing, and holography. In this article, we have presented the results of some experimental studies aimed at quantifying the photorefractive response of several liquid crystal/dye systems, and their dynamics. This is a first step in an attempt to classify these systems, and elucidate the role played by the dye/nematic interactions in their photorefractive response.

[1] *Photorefractive Materials and Their Applications*, edited by P. Gunter and J.-P. Huignard (Springer, Berlin, 1988, 1989), Vols. I and II.
[2] R. M. Herman and R. J. Serinko, Phys. Rev. A **19**, 1757 (1979).
[3] B. Ya. Zel'dovich, N. F. Pilipetski, A. V. Sukhov, and N. V. Tabiryan, JETP Lett. **31**, 263 (1980).
[4] S. D. Durbin, S. M. Arakelian, and Y. R. Shen, Phys. Rev. Lett. **47**, 1411 (1981); Opt. Lett. **6**, 411 (1981).
[5] I. C. Khoo, S. L. Zhang, and S. Shepard, Appl. Phys. Lett. **39**, 937 (1981).
[6] I. C. Khoo, Phys. Rev. A **23**, 2077 (1981); **25**, 1636 (1982).
[7] G. P. Wiederrecht, B. A. Yoon, and M. R. Wasielewski, Science **270**, 1794 (1995).

[8] P. G. de Gennes, *The Physics of Liquid Crystals* (Clarendon, Oxford, 1974).
[9] G. P. Wiederrecht, Annu. Rev. Mater. Res. **31**, 139 (2001).
[10] I. Janossy, A. D. Lloyd, and B. S. Wherrett, Mol. Cryst. Liq. Cryst. **179**, 1 (1990).
[11] I. Janossy, L. Csillag, and A. D. Lloyd, Phys. Rev. A **44**, 8410 (1991).
[12] I. Janossy and T. Kosa, Opt. Lett. **17**, 1183 (1992).
[13] I. C. Khoo, H. Li, and Y. Liang, IEEE J. Quantum Electron. **29**, 1444 (1993).
[14] I. Janossy, Phys. Rev. E **49**, 2957 (1994).
[15] L. Marrucci and D. Paparo, Phys. Rev. E **56**, 1765 (1997).
[16] I. Janossy and L. Szabados, Phys. Rev. E **58**, 4598 (1998).
[17] I. Janossy, J. Nonlinear Opt. Phys. Mater. **8**, 361 (1999).
[18] F. Simoni, *Nonlinear Optical Properties of Liquid Crystals and Polymer Dispersed Liquid Crystals* (World Scientific, Singapore, 1997).
[19] See, for example, P. Yeh, *Introduction to Photorefractive Nonlinear Optics* (Wiley, New York, 1993).
[20] I. C. Khoo, Opt. Lett. **20**, 2137 (1995).
[21] A. Grunnet-Jepson, C. L. Thompson, R. J. Twieg, and W. E. Moerner, J. Opt. Soc. Am. B **15**, 901 (1998).
[22] K. Meerholz, R. Bittner, and Y. D. Nardin, Opt. Commun. **150**, 205 (1998).
[23] L. M. Blinov, *Electro-Optical and Magneto-Optical Properties of Liquid Crystals* (Wiley, Chichester, 1983), Chap. 5.
[24] I. C. Khoo, IEEE J. Quantum Electron. **32**, 525 (1996).
[25] D. Paparo, P. Maddalena, G. Abbate, E. Santamato, and I. Janossy, Mol. Cryst. Liq. Cryst. **251**, 73 (1994).
[26] T. Kosa and I. Janossy, Opt. Lett. **20**, 1230 (1995).
[27] E. Santamato, G. Abbate, P. Maddalena, L. Marrucci, D. Paparo, and E. Massera, Mol. Cryst. Liq. Cryst. **302**, 111 (1997).
[28] L. Marrucci, D. Paparo, P. Maddalena, E. Massera, E. Prudnikova, and E. Santamato, J. Chem. Phys. **107**, 9783 (1997).
[29] V. Kondilenko, V. Markov, S. Odulov, and M. Soskin, Opt. Acta **26**, 239 (1979).
[30] Ph. Refregier, L. Solymar, H. Rajbenbach, and J.-P. Huignard, J. Appl. Phys. **58**, 45 (1985).
[31] M. Z. Zha, P. Amrhein, and P. Gunter, IEEE J. Quantum Electron. **26**, 788 (1990).
[32] K. Sutter and P. Gunter, J. Opt. Soc. Am. B **7**, 2274 (1990).
[33] K. Sutter, J. Hulliger, and P. Gunter, Solid State Commun. **74**, 867 (1990).
[34] T. V. Galstian, B. Saad, and M.-M. Denariez-Roberge, IEEE J. Quantum Electron. **34**, 790 (1998).